Institute of Paper Science and Technology
Atlanta, Georgia

IPST Technical Paper Series Number 678

Hydrodynamics of Dispersed Liquid Droplets in Agitated Synthetic Fibrous Slurries

F. Bose, S.M. Ghiaasiaan, and T.J. Heindel

August 1997

Submitted to
Industrial & Engineering Chemistry Research

INSTITUTE OF PAPER SCIENCE AND TECHNOLOGY
PURPOSE AND MISSIONS

The Institute of Paper Science and Technology is a unique organization whose charitable, educational, and scientific purpose evolves from the singular relationship between the Institute and the pulp and paper industry which has existed since 1929. The purpose of the Institute is fulfilled through three missions, which are:

- to provide high quality students with a multidisciplinary graduate educational experience which is of the highest standard of excellence recognized by the national academic community and which enables them to perform to their maximum potential in a society with a technological base; and
- to sustain an international position of leadership in dynamic scientific research which is participated in by both students and faculty and which is focused on areas of significance to the pulp and paper industry; and
- to contribute to the economic and technical well-being of the nation through innovative educational, informational, and technical services.

ACCREDITATION

The Institute of Paper Science and Technology is accredited by the Commission on Colleges of the Southern Association of Colleges and Schools to award the Master of Science and Doctor of Philosophy degrees.

NOTICE AND DISCLAIMER

The Institute of Paper Science and Technology (IPST) has provided a high standard of professional service and has put forth its best efforts within the time and funds available for this project. The information and conclusions are advisory and are intended only for internal use by any company who may receive this report. Each company must decide for itself the best approach to solving any problems it may have and how, or whether, this reported information should be considered in its approach.

IPST does not recommend particular products, procedures, materials, or service. These are included only in the interest of completeness within a laboratory context and budgetary constraint. Actual products, procedures, materials, and services used may differ and are peculiar to the operations of each company.

In no event shall IPST or its employees and agents have any obligation or liability for damages including, but not limited to, consequential damages arising out of or in connection with any company's use of or inability to use the reported information. IPST provides no warranty or guaranty of results.

Hydrodynamics of Dispersed Liquid Droplets in Agitated Synthetic Fibrous Slurries

Feler Bose and S. Mostafa Ghiaasiaan*
George W. Woodruff School of Mechanical Engineering
Georgia Institute of Technology
Atlanta, GA 30332-0405

Theodore J. Heindel
Institute of Paper Science and Technology
500 Tenth Street, N.W., Atlanta, GA 30318

August 5, 1997

Corresponding author:

S. Mostafa Ghiaasiaan
Associate Professor
G. W. Woodruff School of Mechanical Engineering
Georgia Institute of Technology
Atlanta, GA 30332-0405
Phone: (404) 894-3746
Fax: (404-894-3733
E-mail: seyed.ghiaasiaan@me.gatech.edu

Abstract

The hydrodynamic and liquid particle dispersion processes in agitated vessels containing dilute liquid-liquid dispersions, and dilute liquid dispersions in synthetic fibrous slurries, were experimentally studied. A transparent cylindrical vessel 25 cm in height and 15.5 cm in diameter equipped with a six-blade impeller, with geometric proportions representing the Standard Vessel Configuration, was used. The steady-state size distributions of molten wax particles, which constituted 1% by weight of the mixture everywhere, in pure water, and in aqueous slurries with 0.1%, 0.5%, 0.8% and 1.0% consistencies of nylon fibers, were measured using sampling, and microscopic image analyses. The average nylon fiber length and diameter were 6.22 mm and 19.5 μm, respectively.

With pure water the molten wax particle size distributions were spatially homogeneous and bimodal everywhere and confirmed locally isotropic turbulence in the vessel. In tests with fibrous slurries, for fiber consistencies smaller than 1%, the molten wax particle size distributions remained spatially homogeneous and agreed with the locally isotropic turbulence assumption. However, they were unimodal everywhere with narrow particle diameter spectra. Increasing the fiber consistency and impeller speed both lead to smaller mean molten wax particles and narrower particle diameter ranges, suggesting that fibers hamper particle collision and coalescence. With 1% fiber consistency, widespread flow stratification and fiber flocculation took place.

Introduction

Agitated vessels containing fibrous slurries, with and without gas through-flows, are widely used in mineral separation and paper processing. Among the most important aspects of dispersed-phase agitated contractors, mixing tanks and flotation systems is turbulence, since it

crucially affects such processes as the interparticle collisions, coalescence and breakup. In paper pulp mixing, for example, mixing on the fiber scale, which is needed for effective blending and bleaching, can only be achieved by ensuring high turbulence dissipation throughout the vessel (Bennington et al., 1989), and for pulp consistencies in the 2% to 20% range such mixing can be achieved only when the local turbulence dissipation rate, ε, is larger than a critical threshold value, and the threshold value itself is a strong function of pulp consistency (Wahren, 1980; Gullichsen and Harkonen, 1981; Harkonen, 1985). Despite extensive past investigations dealing with agitated vessels containing liquid-liquid dispersions, few published studies have addressed the hydrodynamic characteristics of dilute liquid dispersions in fibrous slurries.

Agitated liquid-liquid dispersions have been extensively studied in the past, and their hydrodynamic characteristics are at least qualitatively well-understood. Kolmogoroff's theory of local isotropic turbulence agrees well with experimental data representing highly turbulent $\left(\mathrm{Re}_I \gtrsim 2x10^4\right)$ stirred-vessel dispersed contractors (Shinar, 1961; Coulaloglou and Tavlarides, 1977; Narsimhan et al., 1979; Tobin et al., 1990). The dispersed-phase droplet size spectra in these systems fall within the inertial zone of the turbulent eddy energy spectrum and are therefore assumed to interact hydrodynamically with the inertial-zone eddies only. The eddy-particle interactions can then be modeled accordingly, leading to semi-analytical models for the representative equilibrium particle diameter (Sauter mean, average, etc.) for dilute mixtures (Shinar, 1961; Brodkey, 1967; Schulze; 1984, Nishikawa et al., 1987). Except for very dilute dispersions, however, particle breakup and coalescence both contribute to the development of the particle size distribution. The dynamics of the dispersed-phase particle distribution can be mathematically represented by the population balance equation (PBE) (Hulburt and Katz, 1964), using the aforementioned isotropic turbulence theory. Particle collision frequencies have been

accordingly modeled and utilized for the numerical solution of the PBE, leading to relatively successful predictions of experimental particle size distributions (Coulaloglou and Tavralides, 1977; Narsimhan et al., 1979; Das et al., 1987; Muralidhar et al., 1988; Tobin et al., 1990; Tsouris and Tavralides, 1994).

Previous studies of turbulence in fibrous slurries have mostly dealt with the drag reducing effect of fibers. The drag-reducing properties of fibrous additives in channel flow has been well-known for decades and have been studied rather extensively in the past (Hoyt, 1972; Radin et al., 1975). For drag reduction, fibrous additives are preferable to polymer additives because, unlike polymers, fibers do not undergo disintegration due to shear. Although the mechanism responsible for drag reduction is not well understood, it is known that only flexible particles with very large aspect ratio have a significant drag-reducing effect, and it has been shown that their effect in channels is mainly in the form of reduction of the rate of momentum transport in the turbulent core, while their effect close to the channel wall is small (Vaseleski and Metzner, 1974; Lee and Duffy, 1976; Sharma et al., 1979; Duffy and Lee, 1978). No systematic study of hydrodynamic characteristics of agitated fibrous slurries has been reported in the past.

The objectives of this investigation are to experimentally study and compare the hydrodynamic characteristics of dilute liquid-liquid and liquid-fibrous slurry dispersions. In particular, we would like to assess the effect of fibers on the dispersed-phase particle size distribution, and assess the applicability of Kolmogoroff's theory of local turbulence isotropy to fibrous slurries. An understanding of the hydrodynamic characteristics of fibrous slurries and their differences with the relatively well understood characteristics of liquids is crucial for the development of relevant mechanistic models. The hydrodynamic characteristics of synthetic fibrous slurries are addressed in this paper.

Experiments

Figure 1 is a schematic of the experimental apparatus. The test section is a stirred tank made of a 4000 mℓ beaker (15.5 cm in diameter and 25 cm in height), equipped with four baffles and a 6-blade impeller. The impeller and baffle geometric dimensions are chosen based on the Standard Vessel Configuration (SVC) (Holland and Chapman, 1966). The impeller is connected to an electric motor with adjustable rotational speed.

A computer-controlled heated plate is placed underneath the test section for maintaining the temperature of the test fluid in the 60 ± 2°C range. The test section is also equipped with four thermocouples, one connected to the aforementioned heated plate, and the others measuring the fluid temperature distribution in the test section.

The top of the test section is covered with a 3.8 cm-thick plastic plate with 12 strategically distributed sampling holes (see Figure 2) through which pipettes can be used for fluid sample extraction. The coordinates of the sampling locations are specified in the forthcoming discussions with $S_{i,j}$, where the index i represents the vertical location of the point, with i = 1, 2 and 3 representing heights above the test section bottom equal to 2.0, 7.9 and 10.8 cm, respectively. The index j represents the radial and azimuthal positions of the sampling point as depicted in Figure 2, where the distances between the radially-arranged rows of holes from the test section centerline are 1.91, 3.2, 4.4, 5.7, and 7.0 cm, respectively. The sampling pipettes are 8 mm in inner diameter with a 2.5 mm mouth opening and are connected to a suction bulb at the opposite end.

Experiments were conducted using warm distilled water and water-synthetic fiber slurries, mixed with a dilute (1% by volume) suspension of molten microcrystalline wax. Poly Vinyl Alcohol was also added to the mixture at a concentration of about 500 PPM, as a suspending

agent. In separate groups of tests the steady-state size distributions of the molten wax particles in various locations in the test section were measured using pure water and synthetic fiber slurries with fiber consistencies (based on dry fiber weight) of 0.1%, 0.5%, 0.8% and 1%.

The microcrystalline wax used in this study (Astor 3040) has a melting temperature of 54°C. Sampling and size distribution measurements were performed by siphoning off 8 mℓ samples of the fluid mixture from the aforementioned sampling locations, rapidly freezing the wax particles via mixing with cold water in a covered dish and obtaining the particle size distribution by image analysis (Shinar, 1961; Nishikawa et al., 1987; Tobin et al., 1990). The image analysis was performed by using a microscope at 80 magnification and obtaining a frozen and filtered video image of the particles. The image was then analyzed and frontal areas and perimeters of all particles in the image were calculated using the software Optimas 4.1 and 5.2 (Optimas Corp., Edmonds, WA). Wax particles with perimeters larger than 31.4 μm, which constituted the bulk of particles in all tests, were all included in the measurements. Wax particles with smaller perimeters were disregarded because, in addition to constituting a very small fraction of all particles, they were often difficult to distinguish from the background in the image analysis. Although these small particles can be important in certain mass transfer processes, their neglection does not impact the major conclusions of this paper, because they represented the lowest end of the particle size distributions, and had a very small effect on the measured size distribution characteristics. Equivalent particle diameters were determined based on particle projected area. Each image analysis typically included more than 1100 particles. The particle size distributions were discretized into a number of size bins for convenience, which are used for depicting the distribution of particle number densities in the forthcoming discussion of the

experimental results. Thus, the number fraction density associated with particle size bin j, which covers equivalent particle diameters in the D_j^- to D_j^+ range, is calculated from

$$f(D_j) = \frac{n_j}{n_{tot}(D_j^+ - D_j^-)} \tag{1}$$

where D_j is the equivalent particle diameter representing size bin j, n_j is the number of particles with equivalent diameters in the D_j^- to D_j^+ range, and n_{tot} is the total number of particles counted. Evidently $D_{j+1}^- = D_j^+$. In the experimental results to be depicted, $D_j = D_j^+$ was assumed, and the size bins represented 10 μm equivalent particle diameter intervals.

The geometric characteristics of the synthetic fibers used in the experiments (Regular Tenacity Nylon 6, Mini Fiber, Inc.) were directly measured. The measured fiber length and diameter distributions are depicted in Figures 3 and 4, respectively. The fiber average length was 6.22 mm, with a standard deviation of 0.37 mm; and the average fiber diameter was 19.5 μm, with a standard deviation of 2.5 μm. Due to their large aspect ratios, these synthetic fibers evidently have strong drag-reducing capability.

Each test started by preparing a mixture with pre-determined constituents, warming up, and maintaining, the mixture temperature at 60 ± 2°C, and running the impeller at the desired rotational speed for at least three hours before taking samples. For each mixture batch, tests with N = 400 RPM were performed first, followed by N = 500, 700 and 900 RPM. By only increasing the impeller speed with each wax-slurry batch, and running the impeller at the new speed at least for two hours before taking data, the development of equilibrium particle size distributions was ensured. Previous experiments have shown that long mixing time periods are necessary for the development of equilibrium particle size distributions, unless coalescence is totally absent

(Konno et al., 1983; Nishikawa et al., 1987). An empirical correlation for the transient Sauter mean droplet diameter variations has been derived by Hong and Lee (1985), according to which, for our tests, three hours should ensure steady-state. We performed separate tests, furthermore, where particle size distributions extracted at different time periods after rotational speed changes were compared, and the results showed that particle size distributions did not change noticeably after three hours. An additional experiment was performed with all mixture constituents, except the wax, to verify that no particles were observed with image analysis due to possible system impurities.

In order to examine reproducibility, each test, and each sampling, were repeated at least three times, and the samples were analyzed separately, and compared. The reproducibility was always excellent, indicating that errors in the sampling procedure were unlikely.

To ensure locally isotropic turbulence in a liquid-liquid dispersion in agitated vessels, $Re_I \gtrsim 10^4$ must be imposed (Rushton, 1952; Shinar, 1961). In the present experiments Re_I, defined based on properties of water, varied in the 3.6×10^4 to 8.1×10^4 range.

Results and Discussions

Experiments With Pure Water. Representative data obtained with pure water (zero synthetic fiber consistency) are presented here. These data will provide a basis for comparison with fibrous slurry data in the forthcoming section. Furthermore, although the literature pertaining to dilute liquid-liquid dispersions and turbulence in agitated vessels is vast (Aiba, 1958; Shinar, 1961; Chen and Middleman, 1967; Mlynek and Resnick, 1972; Rao and Brodkey, 1972; Coulaloglou and Tavlarides, 1977; Narsimhan et al., 1979; Sovova and Prochazka, 1981; Konno et al., 1983; Das et al., 1987; Nishikawa et al., 1987; Laso, et al., 1987; Chatzi and Lee, 1987; Muralidhar and Ramkrishna, 1986; Muralidhar et al., 1988; Tobin et al., 1990; Chatzi et al.,

1991; Tsouris and Tavralides, 1994), some aspects of the dispersion phenomena are not well-understood. Our pure-water data provide new insight into certain aspects of the dispersion process about which previously reported investigations are in disagreement.

Figure 5 depicts the measured wax particle size distributions, obtained in tests with pure water, at the sampling location $S_{2,6}$. The measured size distributions, as will be demonstrated later, were similar in other locations in the test section. The distributions are distinctly bimodal, with the first peak occurring around $D \approx 20$ μm. With increasing the impeller rotational speed, furthermore, the first peak (representing smaller particles) increases in height monotonically, while the second peak shifts towards a smaller size. The first peak equivalent particle diameter, however, appears to be relatively insensitive to the impeller speed.

The bimodality of the dispersed-phase particle size distributions has been reported by only a few investigators in the past (Tobin et al., 1990; Chatzi et al., 1991), and has been overlooked by most investigators, likely due to their crude measurement techniques. Bimodal distributions have been encountered in transient experiments with relatively high dispersed phase concentrations (Tobin et al., 1990; Chatzi et al., 1991), and were attributed by Tobin et al. (1990) to the slow coalescence frequency of smaller particles. The latter authors compared their transient experimental data with four different coalescence frequency models, and observed that the static deformation model proposed earlier by Muralidhar predicted a slight bimodality in the particle distribution, while other models were incapable of predicting it. Our data, however, suggest that bimodal size distributions are a steady-state characteristic of dilute dispersions.

Figure 6 displays the same data as Figure 5, where the wax particle number fraction density function is now presented as a function of dimensionless particle diameter, $\frac{D}{D_{32}}$, with D_{32}

representing the Sauter mean diameter $\left(\sum nD^3 / \sum nD^2\right)$. The size distributions for various impeller speeds shown in Figure 6, as noted, are qualitatively similar. However, they are rather significantly different quantitatively. These quantitative differences are better visible in Figure 7, where data obtained in the same tests as those depicted in Figure 6, and recorded at sampling location $S_{2,8}$ are displayed. Self-similar size distributions have been assumed by some investigators (Narsimhan, 1979; Tobin et al., 1990). These models, in addition to overlooking the aforementioned bimodality of the size distributions, are only approximately valid in their self-similar particle size distribution assumptions.

Figures 8 and 9 compare the wax particle size distributions in four different sampling locations in the test section, measured in tests with N = 500 and 900 RPM, respectively. Evidently, the flow field was relatively homogeneous with respect to the wax particle size distributions (i.e., the dispersions were statistically homogeneous in the vessel). Such spatial homogeneity occurs in highly turbulent dilute dispersions, implies negligible droplet collision rates throughout the pool, and is replaced with increasingly inhomogeneous particle size distributions as the volume fraction of the dispersed phase is increased to a few percent (Park and Blair, 1975). Homogeneously dispersed particle size distributions are also common in transient tests as long as coalescence is insignificant, since the fluid circulation period (typically several seconds in small-scale experiments) is considerably shorter than the time scale of size distribution variations (typically several minutes) (Konno et al., 1988). Particle breakups occur over short time periods, and therefore depend on local turbulence strength (Coulaloglou and Tavralides, 1977; Konno et al., 1983; Narsimhan et al., 1979). Turbulent dissipation, however, is highly nonuniform in agitated vessels. Cutter (1966) noted that in the impeller zone $\frac{\varepsilon}{\overline{\varepsilon}}$ varied

from 70 (at the impeller tip) to about 3.5 near the wall, and outside the impeller zone it could reach as low as $\frac{\varepsilon}{\overline{\varepsilon}} \approx 0.28$. Since homogeneous particle size distributions represent high turbulence intensity regions, the breakup calculations in mechanistic models should be based on turbulence intensities much higher than $\overline{\varepsilon}$ (Narsimhan et al., 1979). Konno et al. (1983) have shown that, at least for transient breakup dominated dispersions $\overline{\varepsilon}$ may not be an adequate scale-up criterion. Nevertheless, empirical and semi-analytical particle size correlations have usually assumed that the $\frac{\varepsilon}{\overline{\varepsilon}}$ distributions are self similar in geometrically-similar systems, and include $\overline{\varepsilon}$ without explicitly addressing spatial distribution of ε.

Kolmogoroff's theory of local isotropic turbulence has been found to agree with various experimental data representing dispersion in highly turbulent stirred-tank contactors (Shinar, 1961; Coulaloglou and Tavlarides, 1977; Narsimhan et al., 1979; Hong and Lee, 1985; Tobin et al., 1990), as well as flotation devices (Schulze, 1984). The break-up of dispersed-phase particles in these systems generally depends on a critical Weber number, and the particle size spectrum is primarily within the inertial turbulent eddy size range. Using theoretical arguments based on Kolmogoroff's theory of local isotropic turbulence, Shinar (1961) derived the forthcoming eqs. 2 and 3 for breakup- and coalescence-dominated regimes, respectively:

$$D_{32}/D_I = C_1\, We_I^{-0.6} \tag{2}$$

$$D_{32}/D_I = C_2\, We_I^{-0.375} \tag{3}$$

where

$$We_I = \rho_L N^2 D_I^3 / \sigma \tag{4}$$

The powers of We_I in the above correlations are determined by locally isotropic turbulence theory, and are retained by most investigators, even in empirical correlations of data. Parameters

C_1 and C_2 appear to be system-dependent, however. Noting the apparent dependence of parameters C_1 and C_2 on properties of the continuous phase, as well as on the concentration of the dispersed phase, some investigators have attempted to empirically correlate C_1 and C_2 accordingly (Nishikawa et al., 1987; Hong and Lee, 1985; Laso et al., 1987). Narsimhan et al., (1979) suggested $C_1 = 0.0530$. Nishikawa et al., (1987) correlated C_1 and C_2 in terms of the viscosities of both the dispersed and the continuous phases, the volume fraction of the dispersed phase, as well as the dimensionless input power defined as:

$$N_P = \frac{P}{\rho_L N^3 D_I^5} \tag{5}$$

Their correlation, when compared with particle sizes reported by several other investigators, however, provided rather poor predictions (Nishikawa et al., 1987). Based on data representing five different liquid-liquid dispersion systems, Hong and Lee (1985) suggested:

$$C_1 = 0.05\,(1+2.316\phi)\,(D_I / D_T)^{-0.75}\, Fr^{-0.13} \tag{6}$$

where the impeller Froude number is defined as:

$$Fr = \rho_L\, D_I^2 N^2 / (gH|\Delta\rho|) \tag{7}$$

An empirical correlation derived by Laso et al. (1987) includes We_I with a power of -0.4, and appears to be appropriate for high concentrations of dispersed phase where break-up and coalescence processes are both important.

Figure 10 depicts the variation of the Sauter mean diameter, D_{32}, as a function of We_I. The data, while confirming the spatial homogeneity of the particle size distributions in the stirred vessel, well conform to eq. 2 with $C_1 = 0.0424$. The root mean square of the deviations of the experimental data from eq. 2 with the aforementioned value for C_1 is 5.8 μm. Predictions of eq. 3, with $C_2 = 0.0128$ are also depicted in Figure 10, for which the root mean square of deviations

(which have been minimized with the latter choice of C_2) is 10.0 μm. Local isotropic turbulence, and breakup-dominated particle size distribution assumptions are thus valid. The empirical correlation of Hong and Lee (1985), eq. (6), on the other hand, significantly over predicts the data.

Experiments with Fibrous Slurries. Figures 11, 12 and 13 display typical wax particle size distributions measured at two sampling locations ($S_{2,6}$ and $S_{2,8}$), obtained with 0.1%, 0.5% and 0.8% fiber consistencies, respectively. With 0.1% and 0.5% consistencies the depicted impeller speeds are in the 400 RPM to 900 RPM range. With 0.8% consistency, however, large scale flocculation and poor mixing could be observed in the test section when N<500 RPM, and therefore wax size distributions are displayed for $500 \leq N \leq 900$ RPM. For all combinations of fiber consistency and impeller speed the wax particle size distributions were spatially homogeneous (i.e., the wax particle properties were statistically homogeneous in the vessel). The size distributions are depicted in Figures 11-13 only for two sampling locations, $S_{2,6}$ and $S_{2,8}$, for clarity. Spatial homogeneity, however, was confirmed by similar size distributions representing all sampling locations and indicated that similar to the aforementioned pure water tests, the slurries all remained well-mixed in the experiments.

Unlike the pure water data, the wax particle size distributions in the slurries depicted in Figures 11-13, except for data representing 0.1% consistency and N=400 RPM, are essentially unimodal, and cover relatively narrow spectra: 10-80 μm in the 0.1% consistency tests, 10 - 70 μm in the 0.5% consistency tests, and 10-50 μm with 0.8% consistency. The wax particle size distributions in the pure water tests (see Figures 5 and 6) typically covered the 10 - 200 μm range. The data for N=400 RPM and 0.1% fiber consistency shown in Figure 11 are clearly

bimodal, and a comparison between the latter figure and Figure 5 shows that the presence of fibers has mainly affected the second mode's location on the spectrum, reducing its corresponding particle diameter significantly. The size distributions in the fibrous slurries are sensitive to the impeller rotational speed, N, and with increasing N they monotonically shift to the left (i.e., smaller particles) and become distinctly narrower. Furthermore, at least in the consistency range tested, the wax particles become monotonically smaller, and their size distributions become narrower, as the fiber consistency is increased. These narrow wax particle size distributions at high fiber consistency and high impeller speed appear to be qualitatively different than previously reported dispersed phase size distributions in liquid-liquid dispersions. For the 0.5% consistency slurry and N = 900 RPM, for example, the wax particle size distribution covers the remarkably narrow 20 - 40 μm range. For the 0.8% consistency and N = 900 RPM the wax particles are approximately monodisperse with $D \approx 20$ μm. (Note that size bins covering 10 μm diameter ranges have been utilized, and see eq. 1 and its corresponding discussion.)

The unimodality and the relative absence of large wax particles in the tests with fibrous slurries can be at least partially attributed to the prevention of wax particle collision and coalescence by the fibers. In pure water (zero fiber consistency) dispersions with low dispersed phase concentration, the dispersed-phase interparticle collisions and coalescence, although small, may not be totally absent and can be responsible for the observed presence of relatively large particles and the second mode in the equilibrium wax particle size distribution (see Figures 5 and 6). The presence of long cylindrical fibers can reduce or hinder the dispersed-phase inter-particle collisions, thereby reducing coalescence and eliminating large particles from the particle size spectrum, and hence shifting the location of the second (larger diameter) modes in the particle

size spectra towards the left (i.e., a smaller diameter). The data depicted in Figures 11-13 confirm this argument. With 0.1% fiber consistency and N=400 RPM, considerable reduction of the particle diameter representing the second mode has occurred due to the presence of fibers, while the first mode has undergone little change in comparison with the data representing pure water (see Figure 5). With higher fiber consistencies and/or higher impeller speeds, however, the displacements of the second modes have been so significant as to make them indistinguishable from the first mode, at least within the particle size bins applied here. The above argument, whereby the particle size bimodality is attributed to coalescence is, however, inconsistent with the low concentration of wax in the tests which implies little interparticle collisions. The disappearance/or displacement of the second mode in the wax particle size distribution in fibrous slurries can also be attributed to the wax particle-fiber collisions. The direct effects of fiber particles on the dispersed-phase particle breakup and coalescence are thus not clear and need systematic studies. Indirectly, however, the fibers may reduce the turbulent momentum transport in the slurry, as similar drag-reducing fibers do in the turbulent core of channels (Vaseleski and Metzner, 1974; Sharma et al., 1979; Duffy and Lee, 1978), thereby affecting the dispersed-phase particle size distribution.

Typical measured wax particle size distributions are depicted in Figures 14-16, as functions of the dimensionless particle diameter, $\frac{D}{D_{32}}$. The size distributions were similar at various sampling locations and confirm spatially homogeneous particle size distributions. The size distributions are sensitive to the fiber consistency. At the lowest fiber consistency, 0.1% (Figure 14), the wax particle size distributions are approximately symmetric, with the exception of the data representing N = 400 RPM in which the aforementioned effect of bimodal size distribution

is noticeable. As the fiber consistency is increased, however, the wax particle size distribution is monotonically shifted towards the left, as noted in Figures 15 and 16. The size distributions are, furthermore, sensitive to the impeller rotational speed. The most distinct trend is that at very high impeller rotational speeds the dimensionless size distributions tend to become independent of the rotational speed. This trend is confirmed by the similarity between the size distributions representing N = 700 and 900 RPM in both Figures 14 and 15, and is consistent with the aforementioned mechanism leading to the disappearance of bimodality in the particle size distributions due to fibers. The minimum rotational speed beyond which the dimensionless size distributions become independent of the rotational speed, however, may increase as consistency is increased (see Figure 16).

The variations of the wax particle Sauter mean diameter, D_{32}, as a function of We_I, are depicted in Figure 17, and are curve-fitted using eq. 2 for each fiber consistency. Evidently for all tested consistencies the particle Sauter mean diameters conform to eq. 2, indicating the presence of the isotropic turbulence in the experiments, and confirming that the particle size distributions were predominantly determined by the wax particle breakup. Parameter C_1 is a strong function of fiber consistency, however. For pure water, as mentioned before $C_1 = 0.0424$. With 0.1%, 0.5% and 0.8% consistencies, values of C_1 representing the displayed curves were 0.0194, 0.0123 and 0.011, respectively. Evidently C_1 is a strong function of the fiber concentration in the slurry, and is likely to be a strong function of slurry rheological characteristics as well. It should therefore be modeled or correlated accordingly. Our data, however, are insufficient for this purpose and further systematic studies are needed.

The results of this study indicate that in agitated synthetic fibrous slurries with high Re_I, the assumptions of local turbulence isotropy and spatially-homogeneous dispersed-phase liquid

particle size distribution may be valid. The results also indicate that turbulence and the dispersed phase inter-particle phenomena are significantly affected by the fibers, whereby coalescence may be severely suppressed. Due to their capability for reducing turbulent momentum transport, furthermore, synthetic fibers with large aspect ratio may also affect the dispersed-phase particle breakup phenomena. The existing semi-analytical models for dispersed particle coalescence and breakup phenomena may thus be inappropriate for fibrous slurries. Further studies are thus needed.

The synthetic fibers utilized in this study did not flocculate when fiber consistency was lower than 1%. The results of this study evidently do not apply to fibers which readily flocculate, e.g., paper pulp slurries. The hydrodynamics of pulp slurries need separate investigations.

Conclusions

Turbulence, and the dispersion of a dilute liquid in an agitated vessel containing a pure liquid and fibrous slurries were experimentally studied. Mixtures of warm water and 1% by volume molten wax, and aqueous slurries with 0.1%, 0.5%, 0.8% and 1% consistencies of nylon fibers mixed with 1% by volume molten wax, were used. The agitated cylindrical vessel was 25 cm in height and 15.5 cm in diameter, was equipped with a 6-blade impeller and its geometric proportions represented the Standard Vessel Configuration. In the tests, samples were withdrawn from various locations in the test section, their molten wax particles were immediately frozen and their size distributions were measured using microscopic image analyses. The impeller Reynolds numbers, defined based on water properties, varied in the 3.6×10^4 to 8.1×10^4 range.

The wax particle size distributions in the pure water tests were spatially homogeneous and bimodal everywhere and confirmed locally isotropic turbulence in the vessel. With the fibrous slurries, however, the wax particle size distributions were significantly different. They remained

spatially homogeneous and agreed with the breakup-dominated size distribution predicted by the local isotropic turbulence theory everywhere. They, however, tended to become unimodal as fiber consistency and impeller rotational speed were increased, and represented narrow particle diameter ranges everywhere. Increasing the nylon fiber consistency and impeller speed both lead to monotonic reduction in the mean wax particle size and monotonic reduction in the wax particle diameter range. The existing analytical and semi-empirical models for dispersed particle coalescence and breakup phenomena may thus be invalid for fibrous slurries.

Nomenclature

C_1, C_2 = Dimensionless constants in eqs. 2 and 3.

D = Dispersed-phase equivalent particle diameter, m

D_{32} = Dispersed-phase Sauter mean diameter, m

D_I = Impeller blade diameter, m

D_T = Vessel diameter, m

D_j = Equivalent particle diameter for size bin i

D_j^-, D_j^+ = Lower and upper limits of equivalent particle diameter for size bin j

Fr = Impeller Fronde number defined in eq. 7

f = Particle number fraction density, μm^{-1}

g = Acceleration due to gravity, ms^{-2}

H = Height of liquid in the vessel, m

N = Impeller rotational speed, Hz or RPM

N_p = Dimensionless input power number defined in Eq. 5.

n_j = Number of particles in size bin j

n_{tot} = Total number of particles

P = Input power, W

Re_I = $\rho_L N D_I^2 / \mu_L$ Impeller Reynolds number

$S_{i,j}$ = Sampling location corresponding to height i and radial and azimuthal location j

We_I = Weber number defined in eq. 4.

Greek Letters

ε = Energy dissipation rate, per unit mass, m^2s^{-3}.

$\overline{\varepsilon}$ = Vessel-average value of ε, m^2s^{-3}

μ_L = Dynamic viscosity of the continuous-phase liquid, kg $m^{-1}s^{-1}$

ρ_L = Density of the continuous-phase liquid, kg m^{-3}

$\Delta\rho$ = Density difference between continuous and dispersed phases, kg m^{-3}

σ = Surface tension of the continuous-phase liquid, Nm^{-1}

ϕ = Volume fraction of dispersed phase

Acknowledgment

This research was funded through an IPST/GIT Seed Grant with support from the Member Companies of IPST and the Georgia Tech Research Corporation.

Literature Cited

Aiba, S. Flow Patterns of Liquids in Agitated Vessels. *AIChE J.*, 1958, 4, 485.

Bennington, C.P.J.; Kerekes, R. J.; Grace, J. R. Mixing in Pulp Bleaching. *J. Pulp Pap. Sci.* **1989**, 15, 186.

Brodkey, R. S. *The Phenomena of Fluid Motion;* Addison-Wesley Press: Reading, MA, 1967.

Chatzi, E. G.; Boutris, C. J.; Kiparissides, C. On-Line Monitoring of Drop Size Distributions in Agitated Vessels. 1. Effects of Temperature and Impeller Speed. *Ind. Eng. Chem. Res.*, **1991**, 30, 536.

Chatzi, E.; Lee, J. M. Analysis of Interactions for Liquid-Liquid Dispersions in Agitated vessels. *Ind. Eng. Chem. Res.*, **1987**, 26, 2263.

Chen, H.T.; Middleman, S. Drop Size Distribution in Agitated Liquid-Liquid Systems. *AIChE J.*, **1967**, 13, 989.

Coulaloglou, C. A.; Tavlarides, L. L. Description of Interaction Processes in Agitated Liquid-Liquid Dispersions. *Chem. Eng. Sci.* **1977**, 32, 1289.

Cutter, L. A. Flow and Turbulence in a Stirred Tank. *AIChE J.*, **1966**, 12, 35.

Das, P. Y.; Kumar, R.; Ramkrishna, D. Coalescence of Drops in Stirred Dispersion, A White Noise Model for Coalescence. *Chem. Eng. Sci.*, **1987**, 42, 213.

Duffy, G. G.; Lee, P. F. W. Drag Reduction in the Turbulent Flow of Wood Pulp Suspensions. *Appita*, **1978**, 31, 280.

Gullichsen, J.; Harkonen, E. Medium Consistency Technology. I. Fundamental Data. *TAPPI J.*, **1981**, 64, 69.

Harkonen, E. J. Variables Influencing the Power Consumption in Medium Consistency Mixing, Medium Consistency Seminar, Hollywood, FL, TAPPI Press, Atlanta, Georgia, pp. 45-49, 1985.

Holland, F.A.; Chapman, S.S. *Liquid Mixing and Processing in Stirred Tanks;* Reinhold Publishing Corp.: New York, 1966.

Hong, P.O.; Lee, J. M. Changes of the Average Drop Sizes During the Initial Period of Liquid-Liquid Dispersions in Agitated Vessels. *Ind. Eng. Chem. Process Des. Dev.*, **1985**, 24, 868.

Hoyt, J. W. The Effect of Additives on Fluid Friction. *J. Basic Eng.*, **1972**, 94D, 258.

Hulburt, H. M.; Katz, S. Some Problems in Particle Technology, A Statistical Mechanical Formulation. *Chem. Eng. Sci.,* **1964**, 19, 555.

Konno, M; Aoki, M.; Saito, S. Scale Effect on Breakup Process in Liquid-Liquid Agitated Tanks. *J. Chem. Eng. Jap.*, **1983**, 16, 312.

Konno, K.; Muto, T.; Saito, S. Coalescence of Dispersed Drops in an Agitated Tank. *J. Chem. Eng. Jap.*, **1988**, 21, 335.

Laso, M.; Steiner, L., Hartland, S. Dynamic Simulation of Agitated Liquid-Liquid Dispersions-II. Experimental determination of Breakage and Coalescence Rates in a Stirred Tank. *Chem. Eng. Sci.,* **1987**, 42, 2437.

Lee, P.F. W.; Duffy, G. G. Relationships Between Velocity Profiles and Drag Reduction in Turbulent Fiber Suspension Flow. *AIChE J.,* **1976**, 22, 750.

Mlynek, Y.; Resnick, W. Drop Sizes in an Agitated Liquid-liquid System. *AIChE J.*, **1972**, 18, 122.

Muralidhar, R.; Ramkrishna, D. An Inverse Problem in Agglomeration Kinetics. *J. Colloid Interface Sci.*, **1986**, 112, 348.

Muralidhar, R.; Ramkrishna, D.; Das, P.; Kumar, R. Coalescence of Rigid Droplets in a Stirred Dispersion - II. Band-Limited Force Fluctuations. *Chem. Eng. Sci.,* **1988**, 43, 1559.

Narsimhan, G.; Gupta, J. P.; Ramkrishna, D. A Model for Transitional Breakage Probability of Droplets in Agitated Lean Liquid-Liquid Dispersions. *Chem. Eng. Sci.,* **1979**, 34, 257.

Nishikawa, M.; Mori, F.; Fujieda, S. Average Drop Size in a Liquid-Liquid Phase Mixing Vessel. *J. Chem. Eng. Jap.*, **1987**, 20, 82.

Park, J. Y.; Blair, L.M. The Effect of Coalescence on Drop Size Distribution in an Agitated Liquid-Liquid Dispersion. *Chem. Eng. Sci.,* **1975**, 30, 1057.

Radin, I.; Zakin, J. L.; Patterson, G. K. Drag Reduction in Solid-Fluid Systems. *AIChE J.,* **1975**, 21, 358.

Rao, M. A.; Brodkey, R. S. Continuous Flow Stirred Tank Turbulence Parameters in the Impeller Stream. *Chem. Eng. Sci.*, **1972**, 27, 137.

Rushton, J. H. Mixing of Liquids in Chemical Processing. *Ind. Eng. Chem.*, **1952**, 42, 2931.

Sovova, H; Prochazka, J. Breakage and Coalescence of Drops in a Batch Stirred Vessel-I Comparison of Continuous and Discrete Models. *Chem. Eng. Sci.*, **1981**, 36, 163.

Schulze, H. J. *Physico-Chemical Elementary Processes in Flotation*; Elsevier: Amsterdam, Holland, 1984.

Sharma, R. S.; Seshadri, V.; Malhotra, R. C. Drag Reduction in Dilute Fiber suspensions: Some Mechanistic Aspects. *Chem. Eng. Sci.*, **1979**, 34, 703.

Shinar, R. On the Behavior of Liquid Dispersion in Mixing Vessels. *J. Fluid Mech.,* **1961**, 10, 259.

Tobin, T.; Muralidhar, R.; Wright, H.; Ramkrishna, D. Determination of Coalescence Frequencies in Liquid-Liquid Dispersions: Effect of Drop Size Dependence. *Chem. Eng. Sci.*, **1990**, 45, 3491.

Tsouris, C.; Tavralides, L. L. Breakage and Coalescence Models for Drops in Turbulent Dispersions. *AICh.E. J.*, **1994**, 40, 3 95.

Vaseleski, R. C.; Metzner, A. B. Drag Reduction in the Turbulent Flow of Fiber Suspensions. *AIChE J.*, **1974**, 20, 301.

Wahren, D. Fibre Network Structures in Papermaking Operations. Conf. Paper Sci. Technol., The Cutting Edge, Inc., Inst. Paper Chemistry, Appleton, Wisconsin, 1980.

List of Figures

Figure 17: The effect of impeller Weber number on the wax particle Sauter mean diameter in tests with fibrous slurries.

Fig. 1

Bose, etal.

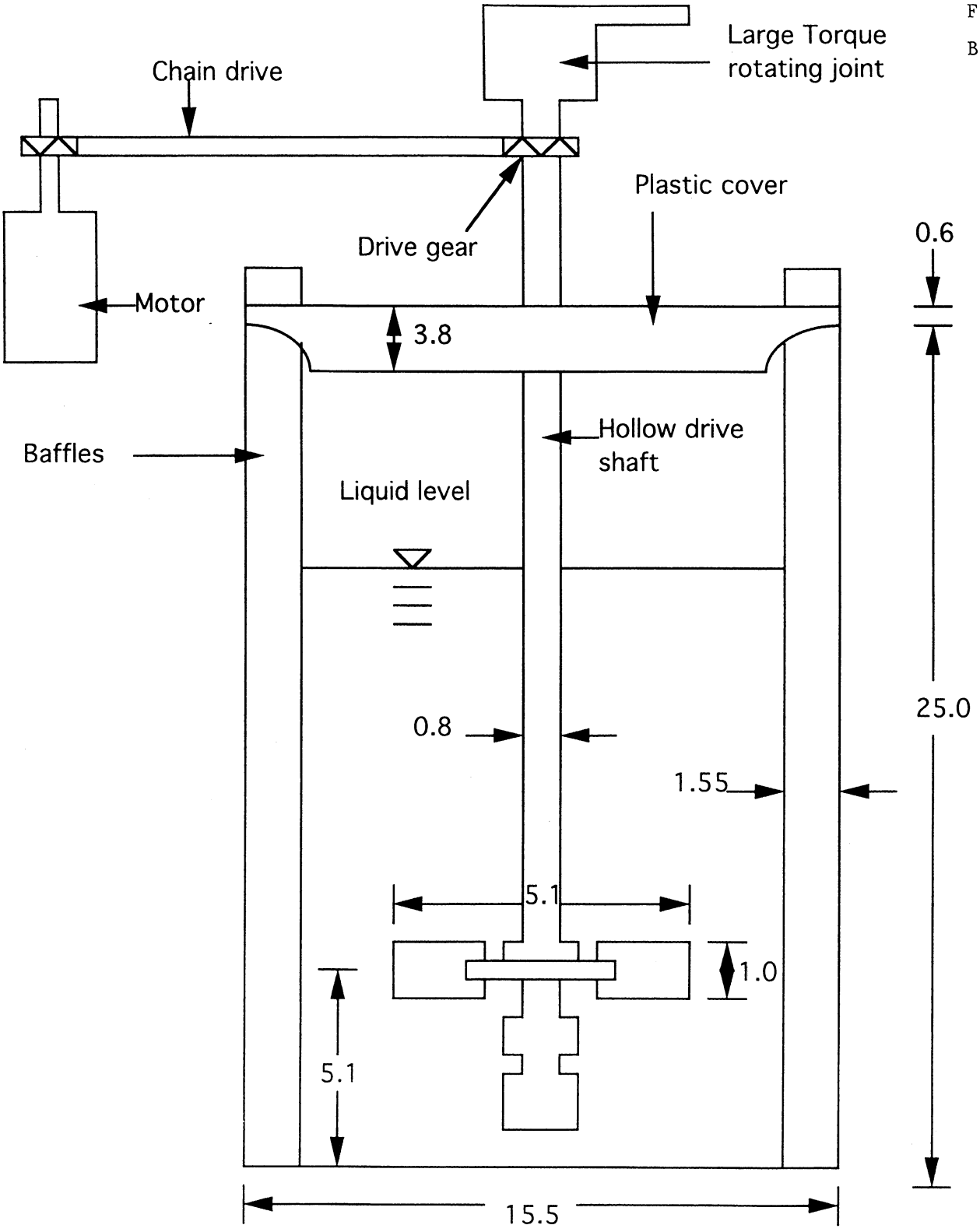

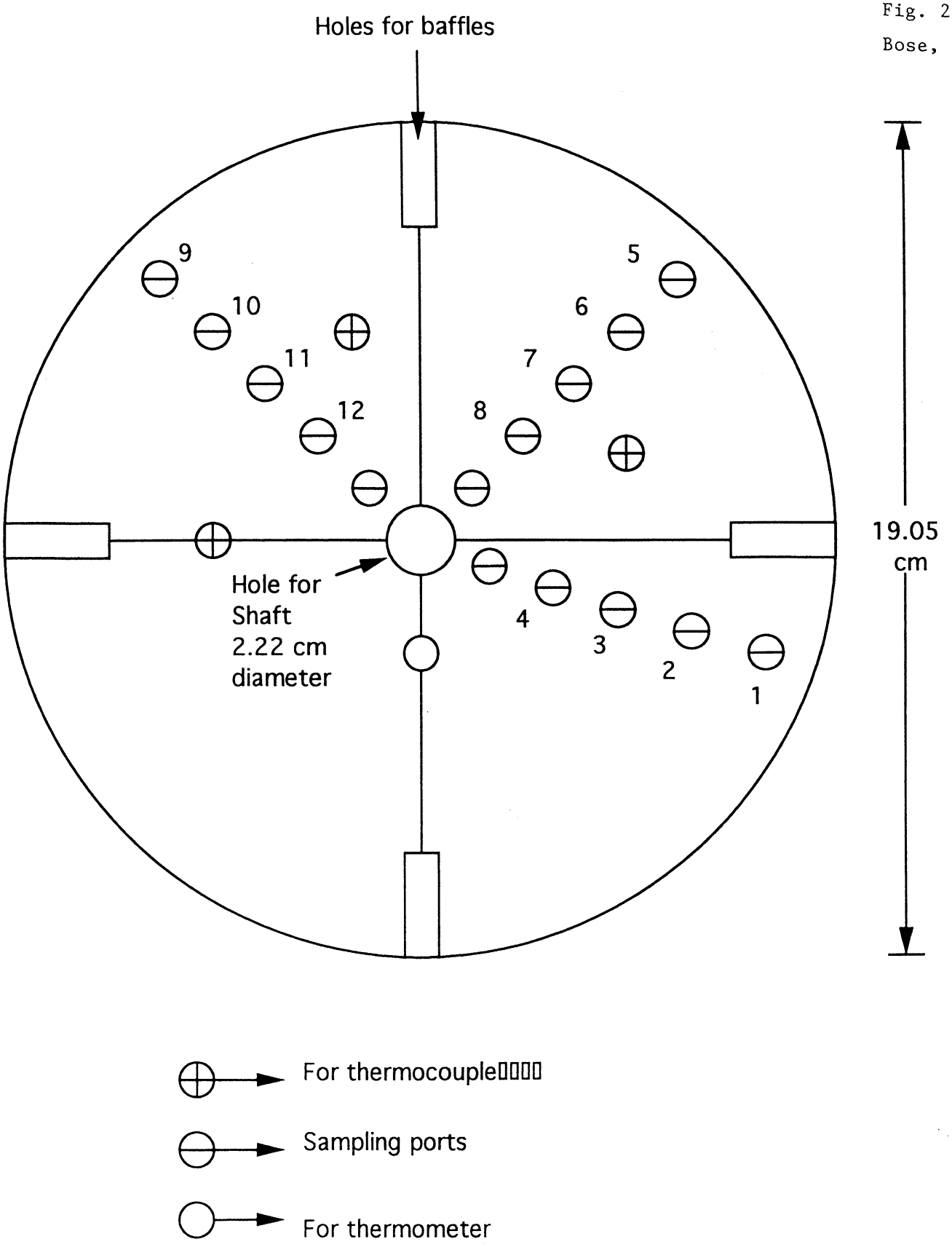

Figure 2: Schematic of the Test Section Cover (not to scale)

Fig. 3

Bose, etal.

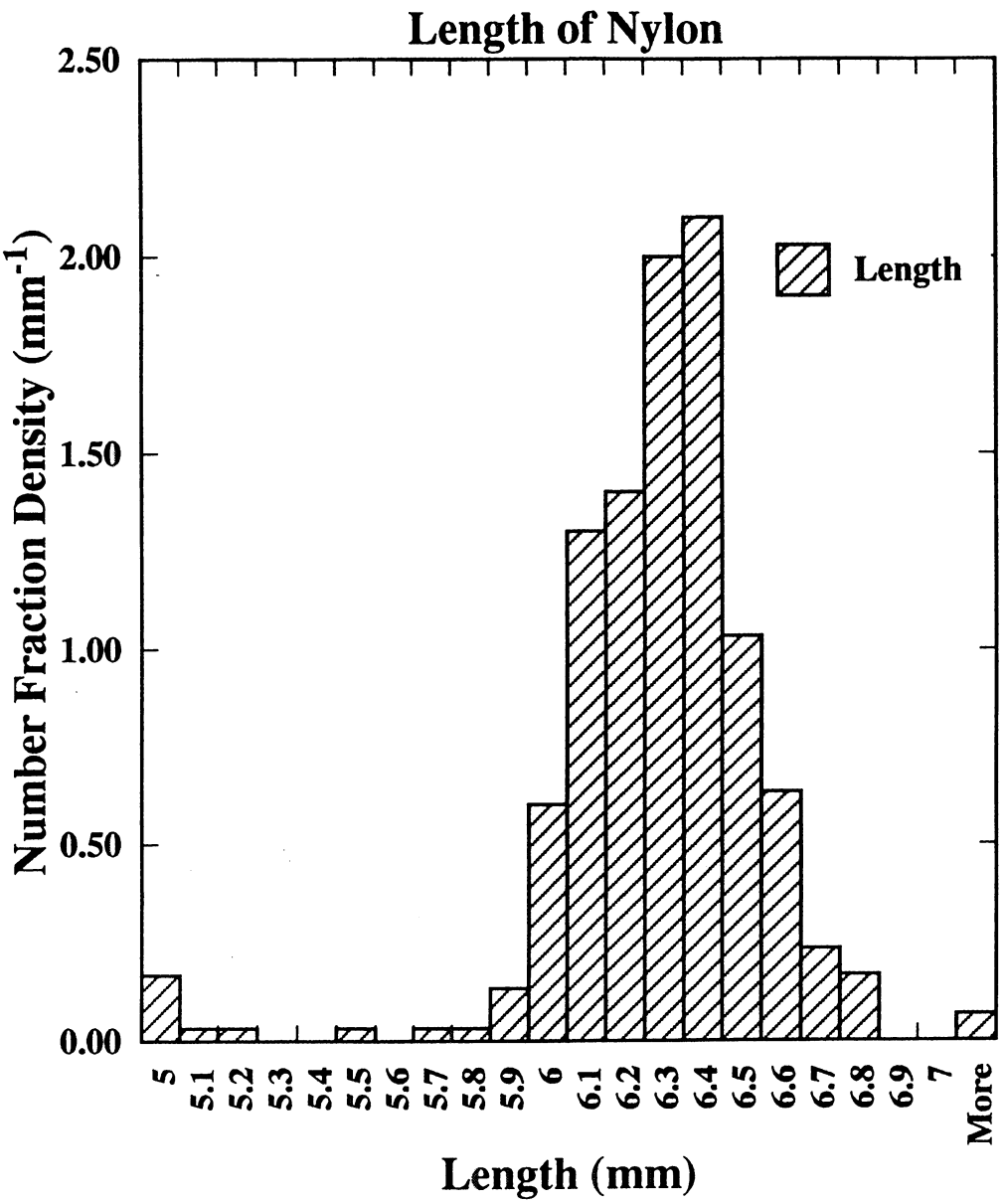

Fig. 4

Bose, etal.

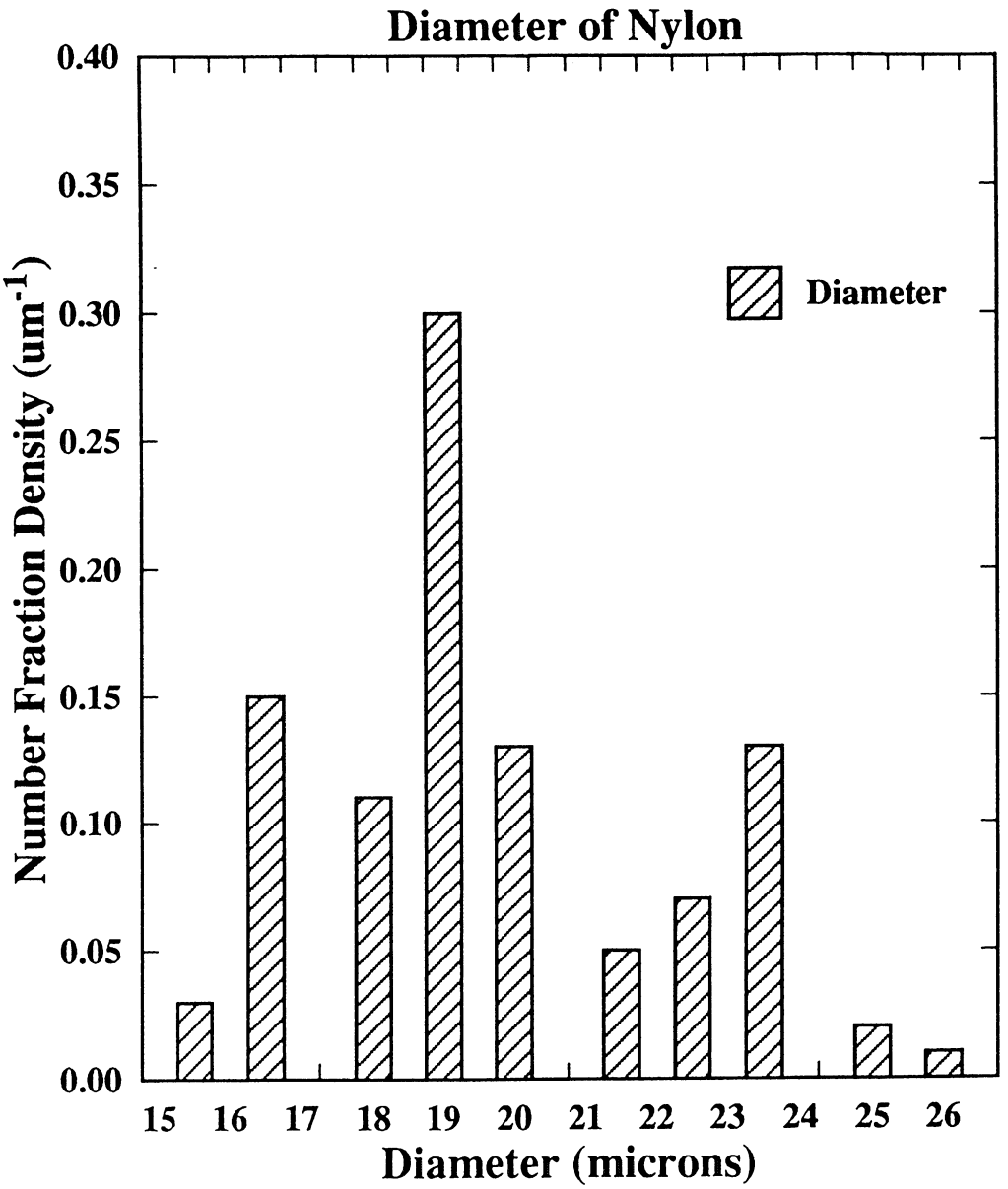

Fig. 5
Bose, etal.

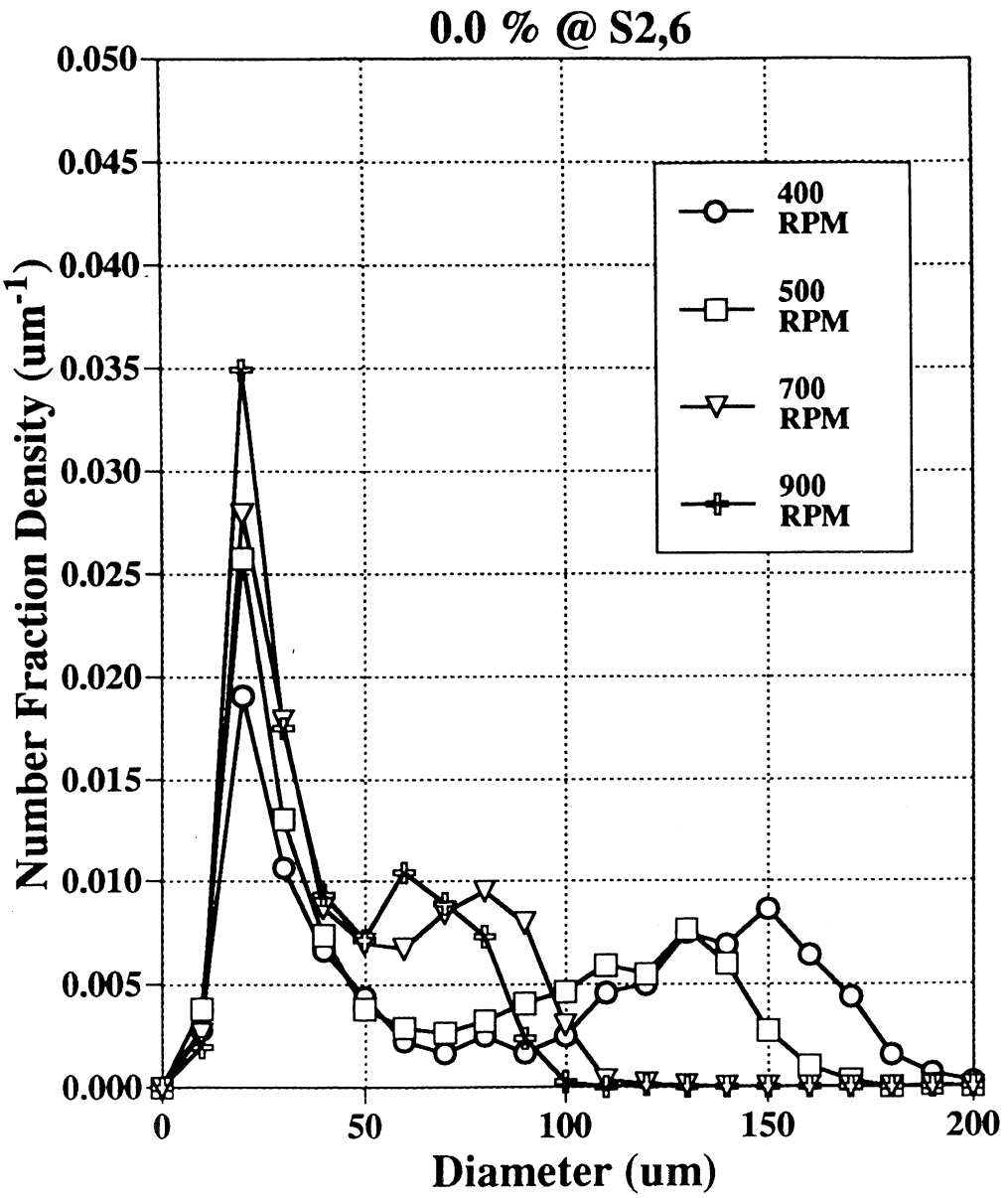

Fig. 6
Bose, etal.

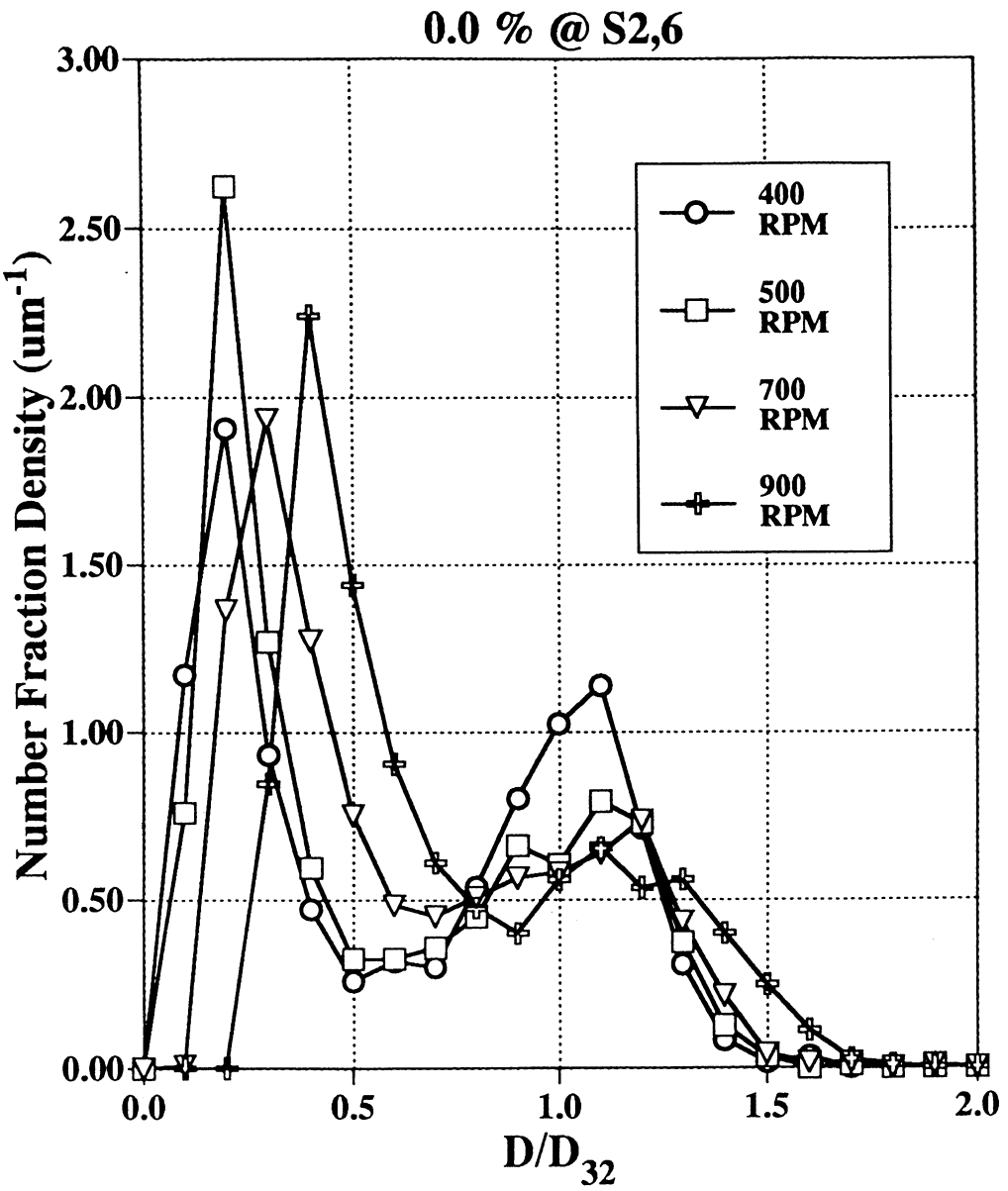

Fig. 7
Bose, etal.

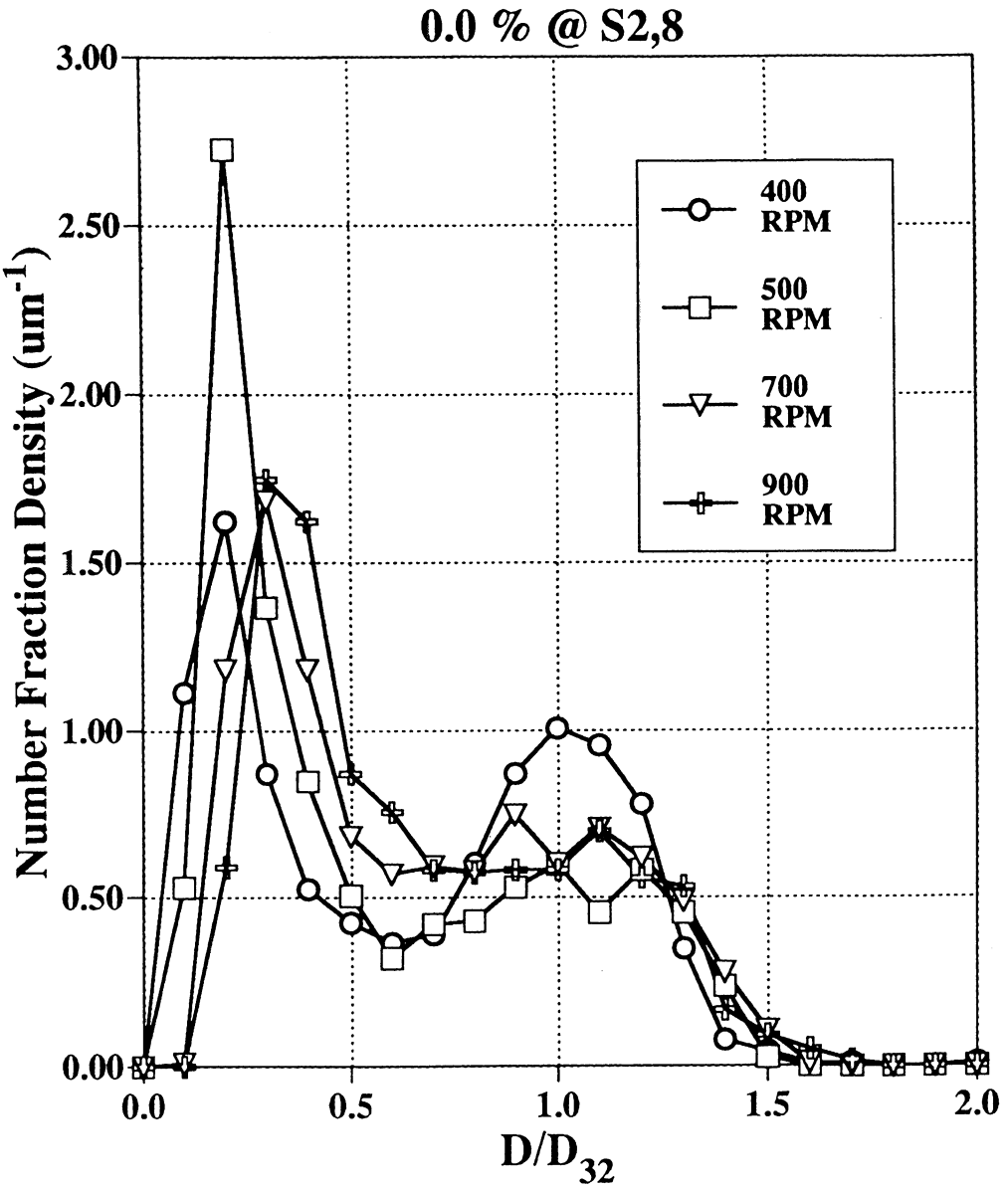

Fig. 8
Bose, etal.

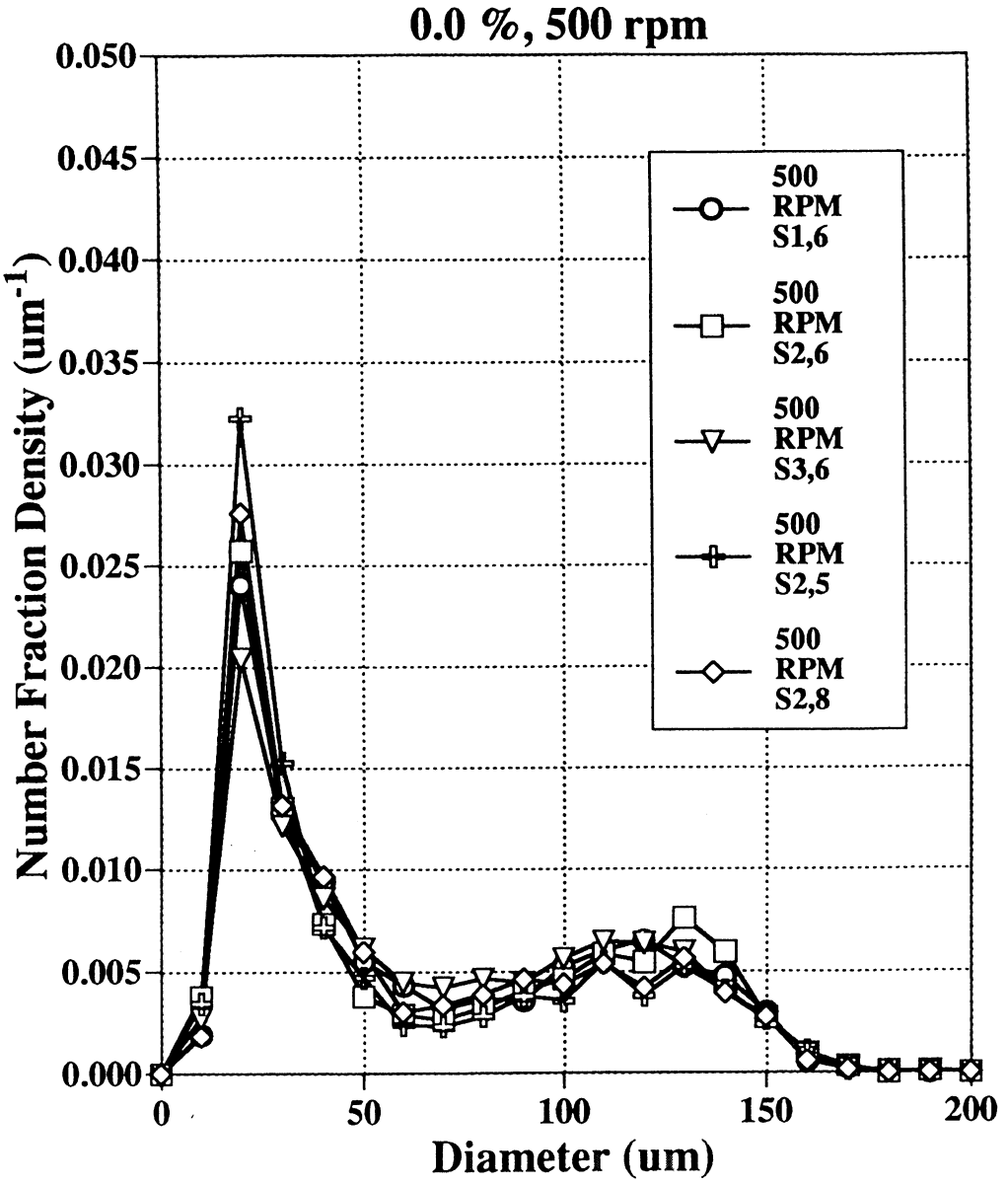

Fig. 9
Bose, etal.

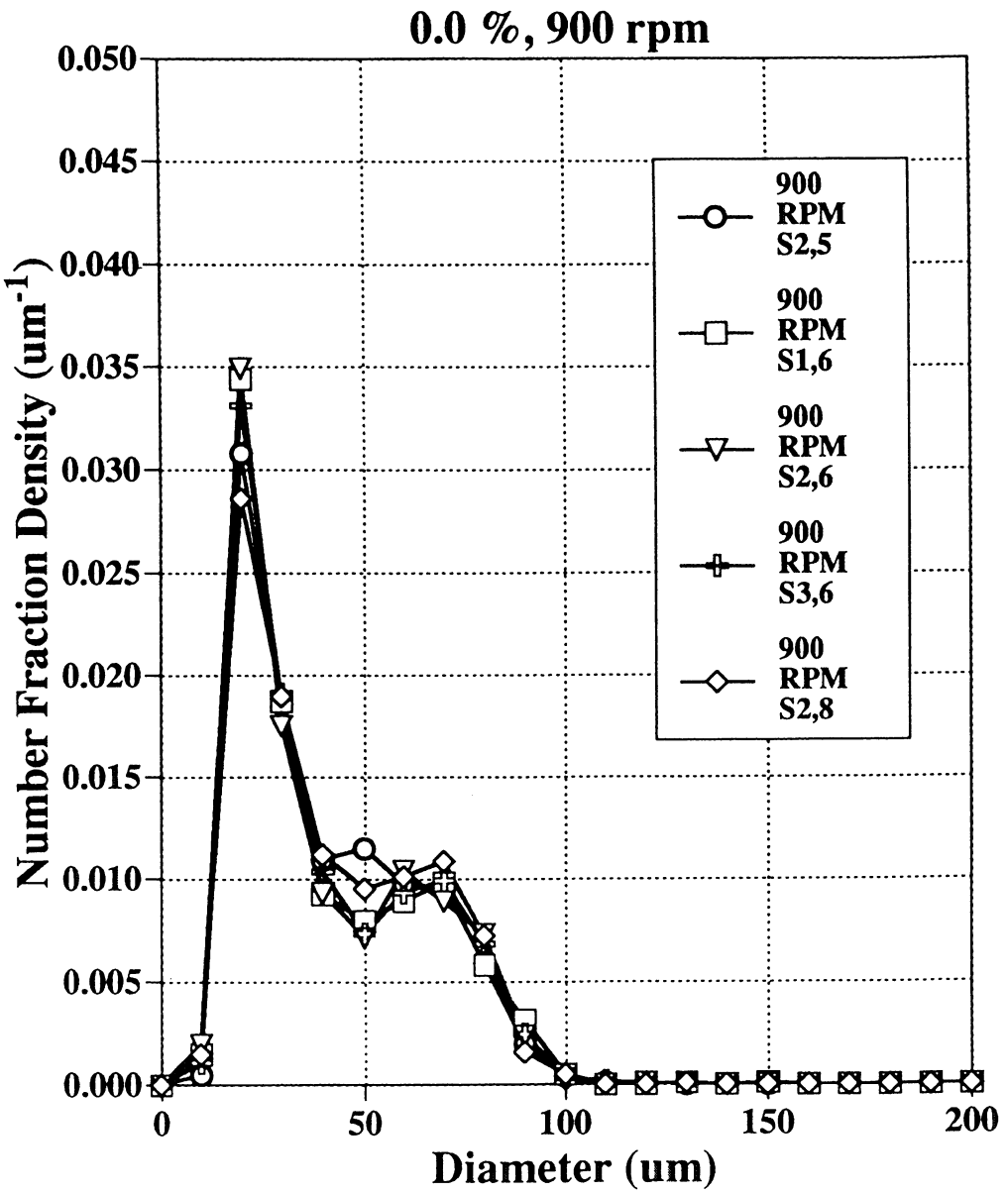

Fig. 10
Bose, etal.

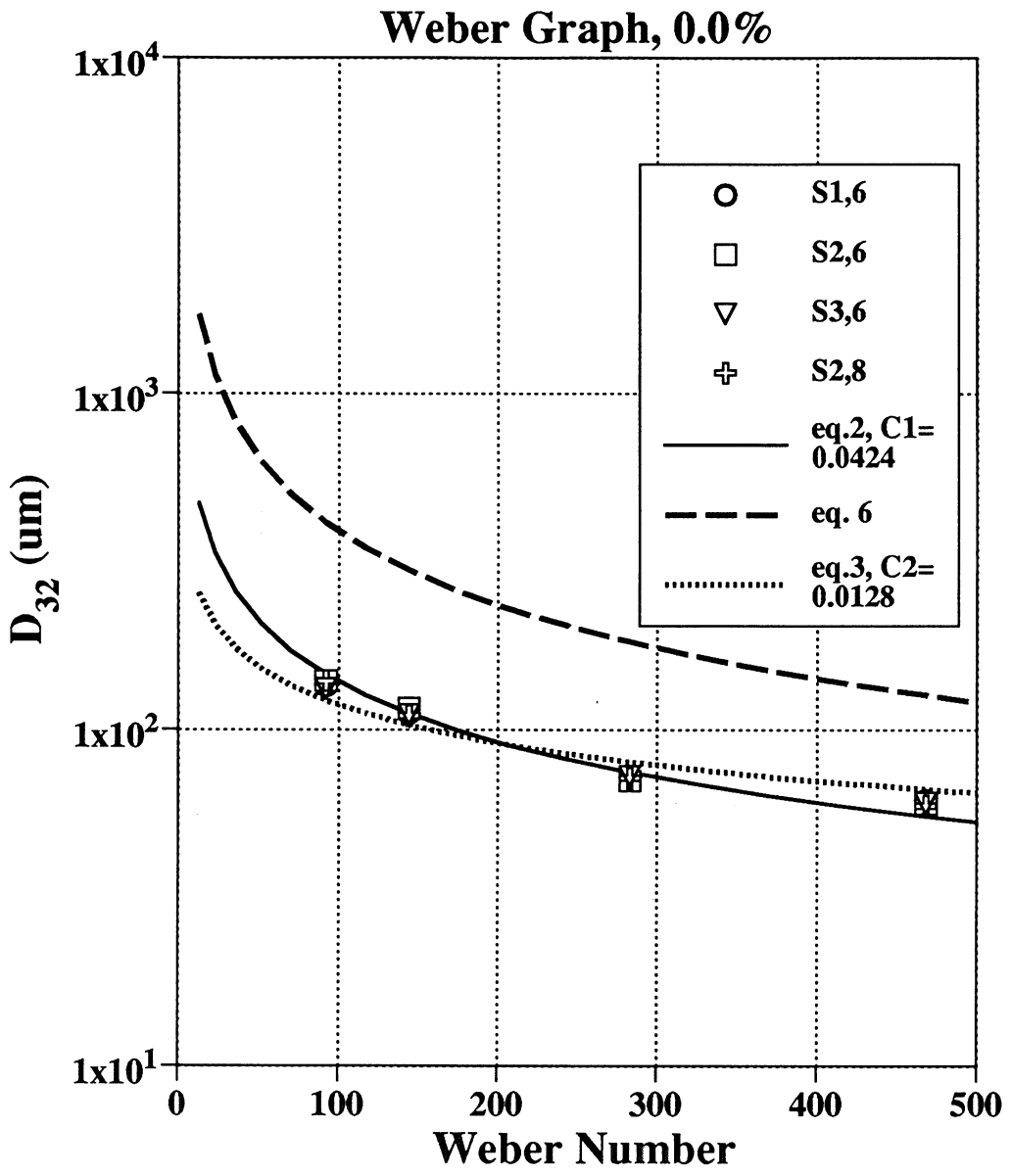

Fig. 11
Bose, etal.

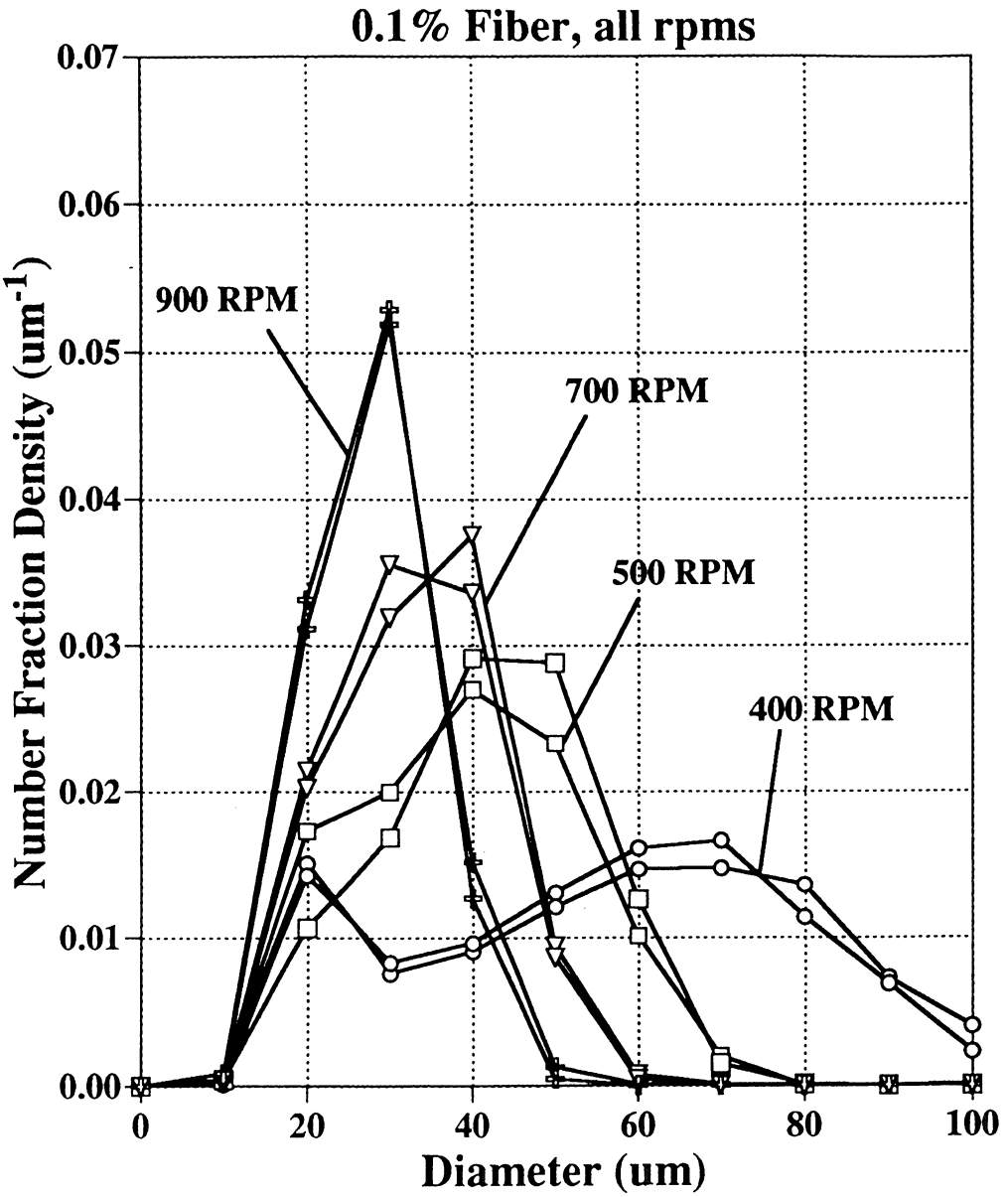

Fig. 12
Bose, etal.

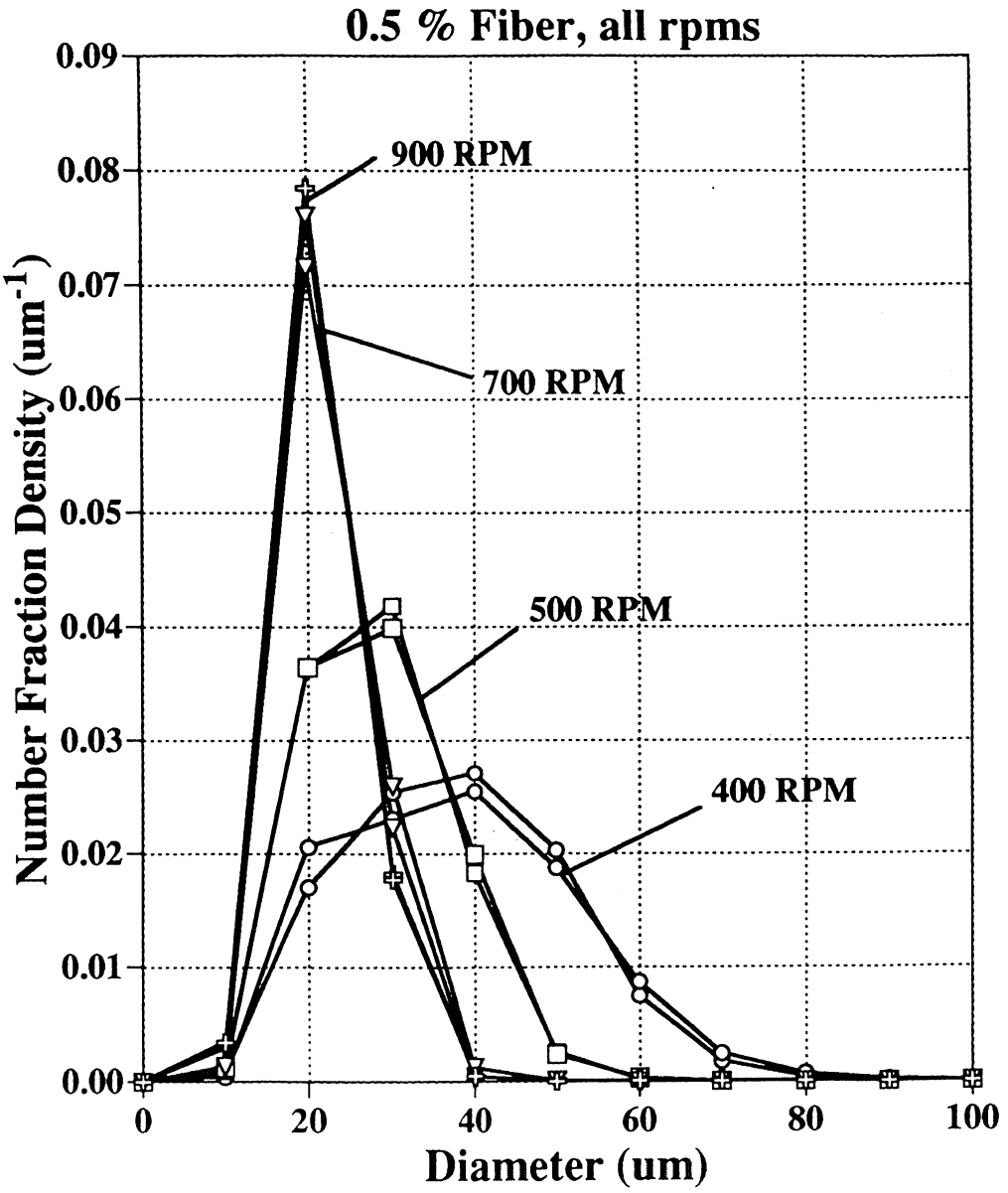

Fig. 13
Bose, etal.

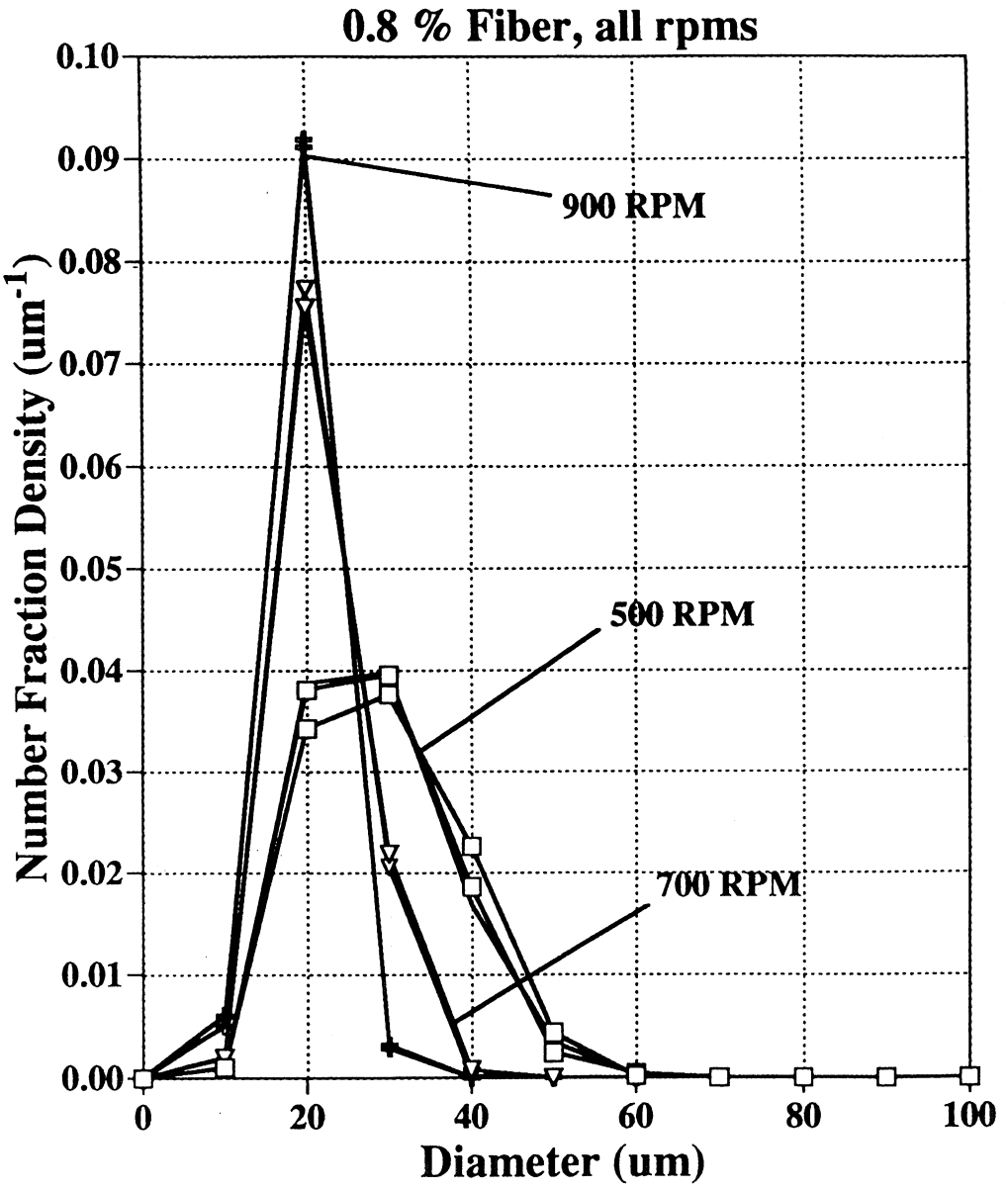

Fig. 14
Bose, etal.

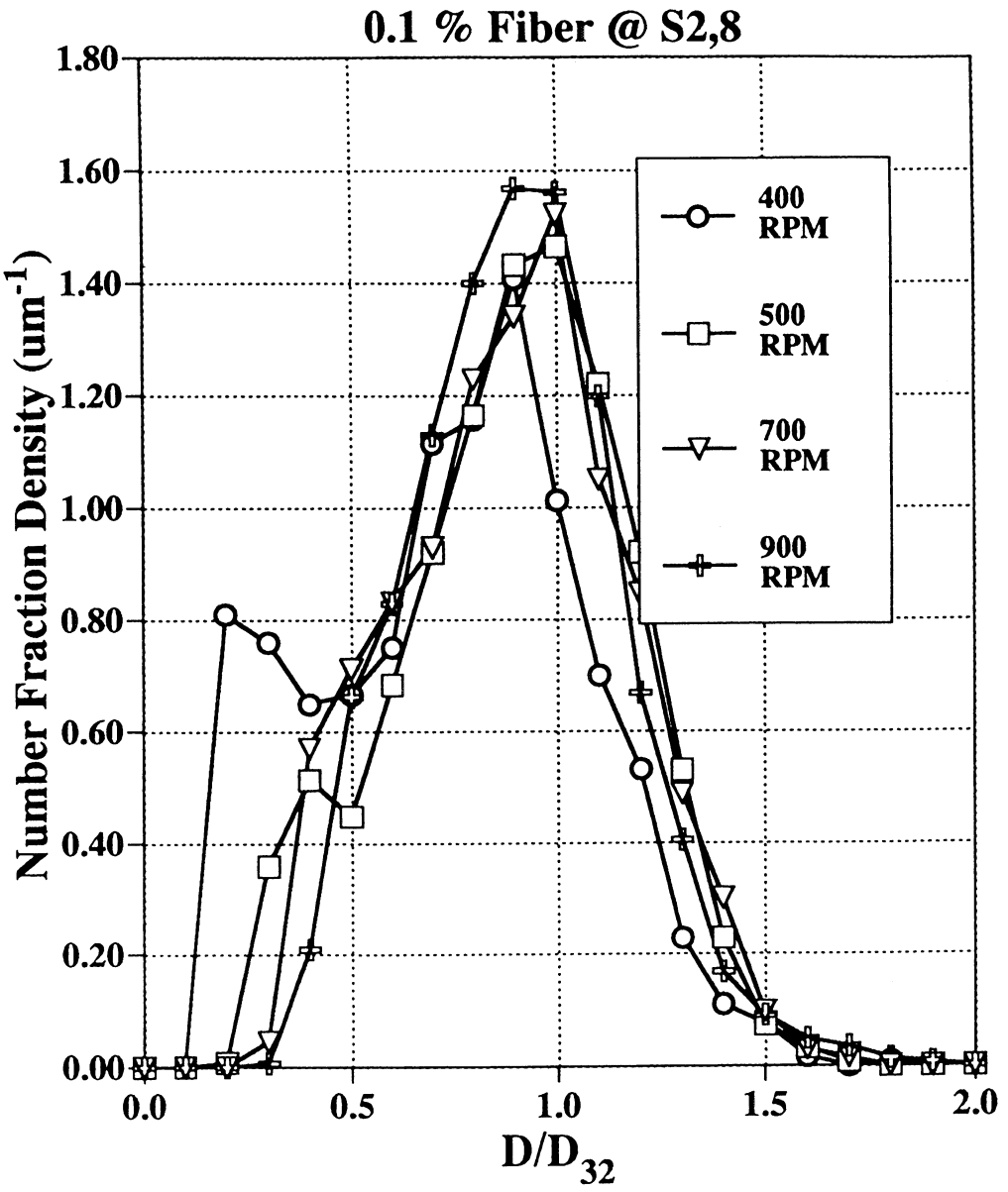

Fig. 15
Bose, etal.

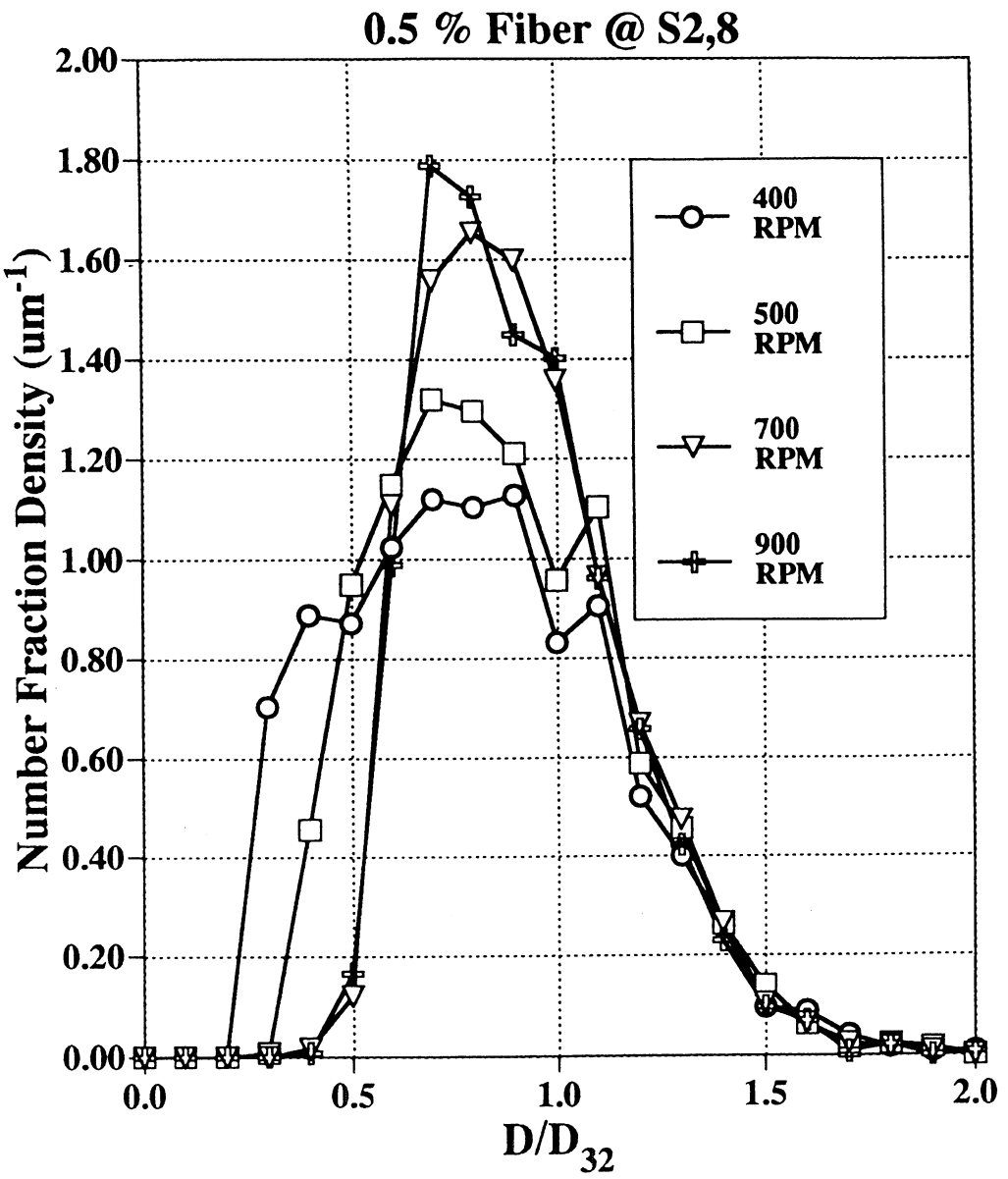

Fig. 16
Bose, etal.

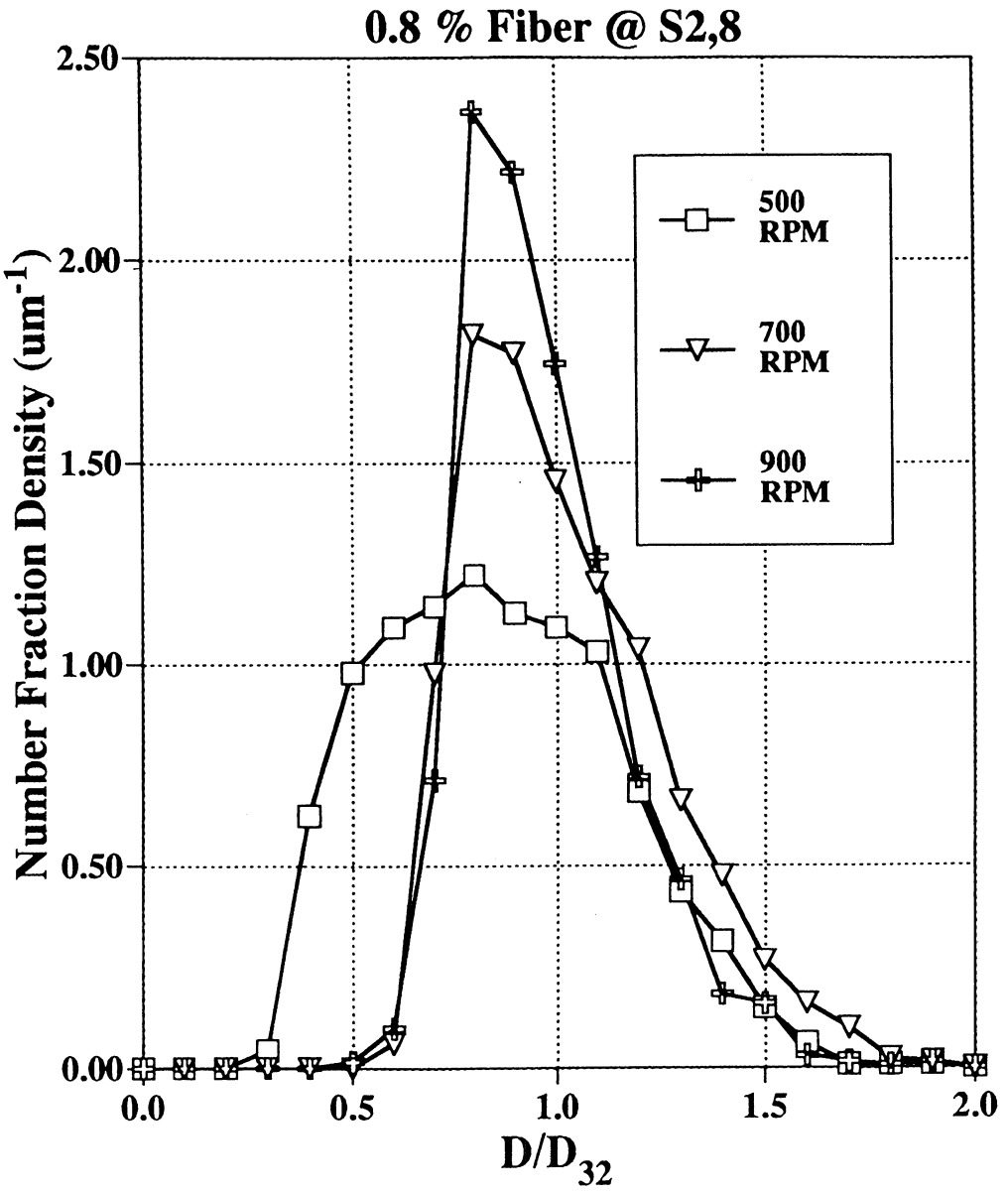

Fig. 17
Bose, etal.